Molecularly imprinted polymers (MIPs) for SARS-CoV-2 omicron variant inhibition: An alternative approach to address the challenge of emerging zoonoses

Marco Dattilo, Francesco Patitucci, Marisa Francesca Motta, Sabrina Prete, Roberta Galeazzi, Silvia Franzè, Ida Perrotta, Mariangela Cavarelli, Ortensia Ilaria Parisi, Francesco Puoci

Colloids and Surfaces B: Biointerfaces 247 (2025) 114408

Contents lists available at ScienceDirect

Colloids and Surfaces B: Biointerfaces

journal homepage: www.elsevier.com/locate/colsurfb

Molecularly imprinted polymers (MIPs) for SARS-CoV-2 omicron variant inhibition: An alternative approach to address the challenge of emerging zoonoses

Marco Dattilo [a,1], Francesco Patitucci [a,1], Marisa Francesca Motta [a], Sabrina Prete [a], Roberta Galeazzi [b], Silvia Franzè [c], Ida Perrotta [d], Mariangela Cavarelli [e], Ortensia Ilaria Parisi [a,f,*], Francesco Puoci [a,f]

[a] Department of Pharmacy, Health and Nutritional Sciences, University of Calabria, Rende, CS 87036, Italy
[b] Department of Life and Environmental Sciences, Marche Polytechnic University, Ancona 60131, Italy
[c] Department of Pharmaceutical Sciences, University of Milan, Milan 20133, Italy
[d] Department of Biology, Ecology and Earth Sciences, University of Calabria, Rende, CS 87036, Italy
[e] Université Paris-Saclay, Inserm, CEA, Center for Immunology of Viral, Auto-immune, Hematological and Bacterial diseases (IMVA-HB/IDMIT), Fontenay-aux-Roses & Le Kremlin-Bicêtre, France
[f] Macrofarm s.r.l., c/o Department of Pharmacy, Health and Nutritional Sciences, University of Calabria, Rende, CS 87036, Italy

ARTICLE INFO

Keywords:
Molecularly Imprinted Polymers (MIPs)
SARS-CoV-2
Spike Protein Receptor-Binding Domain (RBD)
Omicron Variant
Emulsion Polymerization
QCM
Molecular Recognition

ABSTRACT

Emerging zoonoses pose significant public health risks and necessitate rapid and effective treatment responses. This study enhances the technology for preparing Molecularly Imprinted Polymers (MIPs), which function as synthetic nanoparticles targeting SARS-CoV-2 receptor-binding domain (RBD), specifically the Omicron variant, thereby inhibiting its function. This study builds on previous findings by introducing precise adjustments in the formulation and process conditions to enhance particle stability and ensure better control over size and distribution, thereby overcoming the issues identified in earlier research. Following docking studies, imprinted nanoparticles were synthesized via inverse microemulsion polymerization and characterized in terms of size, morphology and surface charge. The selective recognition properties and ability of MIPs to obstruct the interaction between ACE2 and the RBD of SARS-CoV-2 were assessed in vitro, using Non-Imprinted Polymers (NIPs) as controls, and rebinding studies were conducted utilizing a Quartz Crystal Microbalance with Dissipation monitoring (QCM-D). The synthesized nanoparticles exhibited uniform dispersion and had a consistent diameter within the nanoscale range. MIPs demonstrated significant recognition properties and exhibited a concentration-dependent ability to reduce RBD binding to ACE2 without cytotoxic or sensitizing effects. MIPs-based platforms offer a promising alternative to natural antibodies for treating SARS-CoV-2 infections, therefore representing a versatile platform for managing emerging zoonoses.

1. Introduction

The COVID-19 pandemic, caused by the Severe Acute Respiratory Syndrome Coronavirus 2 (SARS-CoV-2), has posed an unprecedented challenge to global public health systems. Emerging in late 2019, the virus rapidly spread worldwide, leading to widespread morbidity and mortality. As of recent records, millions of confirmed cases and deaths have been reported globally, reflecting the virus's severe impact [30]. This worldwide outbreak demonstrated how swiftly emerging infectious diseases can severely impact human health and national economies and underscored the critical need for effective therapeutics, vaccines, and diagnostic tools to combat its transmission and mitigate its impact on public health [18].

A critical component in developing effective targeted interventions is comprehending the structural composition of SARS-CoV-2. The virus's structure comprises several key proteins, including the spike (S) protein, which plays a pivotal role in the virus's ability to infect host cells. The S protein facilitates the virus's entry into host cells by binding to the

* Corresponding author at: Department of Pharmacy, Health and Nutritional Sciences, University of Calabria, Rende, CS 87036, Italy.
E-mail address: ortensiailaria.parisi@unical.it (O.I. Parisi).
[1] ‡ These authors contributed equally

https://doi.org/10.1016/j.colsurfb.2024.114408
Received 12 August 2024; Received in revised form 8 November 2024; Accepted 23 November 2024
Available online 26 November 2024

angiotensin-converting enzyme 2 (ACE2) receptor, a process primarily mediated by the receptor-binding domain (RBD) of the S protein [11]. This interaction is a critical step in the viral infection cycle, making the RBD a prime target for therapeutic interventions.

Vaccines have been instrumental in reducing the severity and spread of the disease, with various types developed, including mRNA, viral vector, and protein subunit vaccines [25]. Monoclonal antibodies have been used as both therapeutic and preventive measures, providing passive immunity by targeting specific viral epitopes [14]. However, the emergence of new variants of concern (VOCs), such as the Delta and Omicron variants, has complicated these efforts due to mutations in the S protein that can alter antibody binding and reduce vaccine efficacy [28].

In particular, during the peak of the pandemic, global concerns surged as the Omicron variant emerged as the most genetically diverse form of SARS-CoV-2 yet known. The B.1.1.529 variant, first detected in Botswana and South Africa, was named as the Omicron variant on November 26, 2021 [29]. Its remarkable ability to spread rapidly and evade immune defenses heightened anxieties worldwide, underscoring the urgent need for a multifaceted approach to interventions, including the development of novel therapeutics [13].

In this context, Molecularly Imprinted Technology (MIT) represents an innovative method that has garnered attention for its role in developing synthetic receptors. Molecularly Imprinted Polymers (MIPs) are synthetic polymers that can be engineered to have specific binding sites, tailored to the shape and chemical properties of target molecules, akin to the binding sites of natural antibodies. This technology offers several advantages, including high stability, ease of production, and the potential for cost-effective mass production. MIPs can mimic natural antibodies' high specificity and affinity, making them promising candidates for various applications, including diagnostics, therapeutic delivery, and environmental monitoring [7,22]. In diagnostics, MIPs can be employed to detect a wide range of analytes, including pathogens, toxins, and biomarkers, with high sensitivity and specificity. This capability is particularly valuable in the context of infectious diseases, where rapid and accurate detection can significantly impact patient outcomes and public health responses [2]. For therapeutic applications, MIPs can be utilized in targeted drug delivery systems, where they can selectively bind to specific sites in the body, releasing therapeutic agents in a controlled manner. This targeted approach can enhance the efficacy of treatments and minimize side effects, offering a significant advantage over conventional therapies [4]. Moreover, MIPs hold potential for the development of next-generation pharmacological agents capable of disrupting protein-protein interactions. In a recent study, Herrera León et al. investigated the application of MIPs as synthetic peptide antibodies targeting Tumor Necrosis Factor-alpha (TNF-α), a cytokine implicated in autoimmune and inflammatory disorders. The proposed inhibition mechanism relies on a highly specific binding process that neutralizes TNF-α's inflammatory effects by blocking its interaction with its cell surface receptors, TNFR1 and TNFR2 [10]. Zhou et al., on the other hand, introduced a potential new application for MIPs in antiviral therapy by using them to inhibit viral infections [31]. Specifically, glycan-imprinted nanoparticles were designed to target the HIV-1 envelope protein. By binding specifically to the glycans on the viral envelope, MIPs were able to prevent HIV-1 from infecting target CD4+ cells. The nanoparticles showed strong binding affinity and high specificity, with broad inhibitory activity against multiple HIV-1 strains. The versatility and adaptability of MIT allow MIPs to be tailored for a broad range of applications, making them a valuable tool in both medical and environmental fields.

Building on this premises, we aimed to apply MIT as a strategy for inhibiting SARS-CoV-2 infection. Several studies have already explored the applicability of MIT for the detection of SARS-CoV-2. For instance, Bajaj et al. investigated the potential of MIPs for detecting the entire SARS-CoV-2 virus using a label-free, miniaturized Surface Plasmon Resonance (SPR) sensor. Their study demonstrated the successful stepwise fabrication of the sensor, indicating its potential role in monitoring and managing viral contamination and infection risks [1]. Raziq et al. focused their attention on the SARS-CoV-2 Nucleocapsid Protein (ncovNP), a key antigen for COVID-19 diagnostics. They developed a portable electrochemical sensor incorporating a poly-m-phenylenediamine-based MIP as a selective recognition element. Validation with clinical nasopharyngeal swab samples demonstrated the sensor's ability to accurately detect ncovNP in complex biological media, showing promising potential for diagnostic applications [24]. Our group recently reported on the development of MIPs capable of selectively recognizing and binding the S protein RBD of SARS-CoV-2, effectively blocking its function and potentially inhibiting viral infection [21]. The MIPs were synthesized via inverse microemulsion polymerization using a non-covalent imprinting approach with acrylamide and methacrylic acid as monomers. In vitro studies confirmed the antiviral activity and specificity of the MIPs. However, challenges such as particle aggregation at high concentrations, reduced stability, and difficulties in controlling particle size and achieving monodispersity were encountered.

Here, we developed a refined synthesis protocol by introducing precise adjustments in the formulation and process conditions, enhancing particle stability, and enabling better control over size and distribution. Additionally, to demonstrate the versatility of the technique, we decided to use the Omicron variant of SARS-CoV-2 as template molecule to reflect ongoing efforts to adapt interventions to emerging viral strains. Various experimental methods, including Dynamic Light Scattering (DLS) for measuring size [12] and gravitational sedimentation with the Turbiscan optical analyzer [16], have been employed to study nanoparticle dispersions. The results showed that MIPs had significantly higher binding efficacy to the RBD compared to non-imprinted polymers (NIPs), due to their specific imprinted cavities. Neutralizing anti-SARS-CoV-2 antibody assay and QCM-D analysis confirmed the superior specificity and binding capability of MIPs, highlighting their potential for precise molecular recognition, outperforming both NIPs and non-target proteins such as Human Serum Albumin (HSA). This technique offers a versatile and effective approach to addressing the evolving challenges posed by SARS-CoV-2 and its variants. By refining synthesis techniques and targeting specific viral components like the RBD, it's possible to enhance the specificity and efficacy of these synthetic particles, potentially leading to new prophylactic and therapeutic options for COVID-19 and other infectious diseases.

2. EXPERIMENTAL SECTION

2.1. Reagents

The receptor-binding domain of the SARS-CoV-2 B.1.1.529 sublineage BA.2 (Omicron) spike protein (RBD, His Tag) was purchased from Sino Biological Inc. (Beijing, China). Acrylamide (AAm), Acrylic acid (AAc), N,N′-methylenebisacrylamide, N-Isopropylacrylamide (NIPAM), n-Propyl Methacrylate (nPMA), N-tert-Butylacrylamide (TBAm), tween-80, span-80, dioctyl sulfosuccinate sodium salt (AOT), ammonium persulfate (APS), N,N,N,N-tetramethylethylenediamine (TEMED), disodium hydrogen phosphate, sodium dihydrogen phosphate, human serum albumin (HSA), 3-sulfo-N-Hydroxysuccinimide (Sulfo-NHS), 1-ethyl-3-(3-dimethylaminopropyl)carbodiimide (EDC), 16-Mercaptohexadecanoic acid (MHA), 11-Mercapto-1-undecanol (MU), Dulbecco's Modified Eagle Medium (DMEM, Product No. D0822), Penicillin/Streptomycin (Product No. P0781), β-Mercaptoethanol (Product No. M3148), Fetal Bovine Serum (FBS, Product No. F4135), Bovine Calf Serum (BCS, Product No. 12133 C), 3-(4,5-dimethylthiazol-2-yl)-2,5-diphenyltetrazolium (MTT, Product No. 475989), nickel sulfate (Product No. 1.06726), propidium iodide (Product No. 537059), FACS buffer (PBS, 0.5–1 % BSA or 5–10 % FBS, 0.1 % sodium azide), sodium azide (Product No. 71289), Bovine Serum Albumin (BSA,

Product No. A4503), and γ-globulin (Product No. G5009) were purchased from Sigma-Aldrich s.r.l. (Milan, Italy). RPMI 1640 medium was obtained from ATCC (Manassas, VA, USA). The Anti-SARS-CoV-2 (BA.2) Neutralizing Antibody Titer Serologic Assay Kit (Catalog number RAS-N087) was obtained from Acro Biosystems (Newark, DE, USA). All solvents were of reagent or HPLC grade and obtained from VWR (Milan, Italy). 5 MHz Au-coated QCM sensors were obtained from Novaetech S.r.l. (Italy).

2.2. Cell cultures

BALB/3T3 cells were purchased from the American Type Culture Collection (ATCC, Manassas, VA, USA) and maintained in DMEM medium (containing 2 mM L-glutamine, 1 % penicillin-streptomycin, and 1 % sodium pyruvate 1 mM) supplemented with 10 % bovine calf serum (BCS) at 37°C in a humidified atmosphere consisting of 5 % CO2 in air. THP-1 cells were purchased from the American Type Culture Collection (ATCC, Manassas, VA, USA) and cultured in RPMI 1640 medium supplemented with 10 % FBS, 1 % Penicillin/Streptomycin, and 0.05 mM β-Mercapto-ethanol at 37°C in a humidified atmosphere consisting of 5 % CO2 in air.

2.3. Instrumentation

Transmission electron micrographs were captured with a Jeol Transmission Electron Microscope, model JEM-1409Plus, operating at 80 kV. The particle size distribution was determined through dynamic light scattering (DLS) utilizing a Zetasizer (Nano-ZS, Malvern Instrument, UK) and Nanoparticle Trafficking Analysis employing a Nanosight NS 300 (Malvern Instrument, UK). For DLS, samples diluted (1:10) in ultrapure water were measured in a disposable cuvette at a detection angle of 173°. ζ-Potential was evaluated on samples placed in a capillary cell. Three measurements were conducted for each sample, and the outcomes are presented as mean and standard deviation. For NTA analysis, samples were diluted in ultrapure water to reach a proper particles/frame value and underwent 5 sequential measurements at 25 °C using a Blue488 laser. The stability studies were carried out using a Turbiscan® DNS™ (Formulaction, Toulouse, France). QCM-D measurements were performed using an openQCM NEXT instrument (Novaetech S.r.l., Italy). Dialysis membranes of 6–27/32" Medicell International LTD (MWCO: 12–14,000 Da) were provided by Spectrum Laboratories Inc., Dalton, U.S.A.

2.4. Computational methods and analysis

SARS-CoV2-RBD Omicron structure was retrieved from Brookhaven Protein Data Bank (uniprot P0DTC2, pdb code 7yow) (http://www.wwpdb.org), was processed within the CHIMERA software [23] and minimized using AMBERff14 force field within AMBER 2020 suite [27].] performing progressive minimizations until the average root mean square deviation of the non–hydrogen atoms reached 0.3 Å. and used in molecular docking calculations. AAm structure was built in and minimized using Gaussian 09 at DFT/6–311 G* level of theory (PubChem CID: 6579) [ref]; the same protocol has been applied to AAc and its conjugate anion acrylate (PubChem CID: 4093), NIPAM (CID: 16637), nPMA (CID: 16638) and TBAm (PubChem CID:7877).

Autodock 4.2/MGLTools 1.5.7 was used to perform the molecular docking calculations [19] using the previously calculated charges at QM/DFT level for the ligands. Particularly we tested the cluster distribution considering different charge types (i.e. Mulliken, NBO), obtaining in the two cases a high correspondence of the clusters' distribution. Initially, a blind docking approach was used in order to identify every putative site on the Receptor Binding Domain (RBD) surface. To predict the probable arrangement of multiple monomer molecules around the protein, a detailed cluster analysis was performed and clusters that fall within the contact surfaces between monomeric chains in the trimeric association of the S protein were excluded from further analysis. Subsequently, on the lowest energy and most populated poses, a focused docking protocol has been applied to better refine both pose and its energy. For the Blind docking, the grid map, cantered in the centre of mass of the enzyme (126x126x126 Å3) included all the RBD surface; in the focused docking protocol, the grid map was centred on the ligand in the considered pose and extended around the cleft (40x40x40 Å3) with points spaced equally at 0.375 Å. The number of GA (genetic algorithm) runs was set to 150, the energy evaluations (25 000 000), the maximum number of top individuals that automatically survive (0.1) and the step size for translation (0.2 Å). All the docking calculations were carried out in triplicate using three different CPUs random seed. The final docked RBD-monomer complexes were ranked according to the predicted binding energy and all the conformations were processed using the built-in clustering analysis with a 2.0 Å cutoff.

2.5. Synthesis of molecularly imprinted particles

Molecularly imprinted particles were synthesized as previously described [21], with minor adjustments.

Briefly, the water phase (1.0 mL), containing functional and cross-linking monomers, was sonicated and mixed with the SARS-CoV-2 receptor-binding domain. The oil phase, comprising deoxygenated hexane (22 mL), AOT (0,8 g), Span-80 (1,69 g), and Tween-80 (0,56 g), was prepared separately. The water phase was transferred into a 1 mL syringe, which was fitted with a 0.5-inch 30 G stainless steel needle. This syringe was then mounted onto a syringe pump (NE-1600, New Era Instruments, USA) to facilitate controlled injection into the oil phase. Using the syringe pump, the water phase was injected into the oil phase at a constant flow rate. The pump was calibrated to regulate this flow rate precisely, which was crucial for the formation of uniform spherical water-in-oil (W/O) droplets. By maintaining controlled flow conditions, we were able to optimize the droplet size and uniformity, thereby enhancing the overall stability and efficiency of the emulsion polymerization process. Polymerization was initiated with 10 % APS solution (100 μL) and TEMED (10 μL), and the reaction mixture was stirred for 2 hours. The resulting polymeric nanoparticles were precipitated with ethanol and washed with various solvents to remove unreacted components, surfactants, and templates. The polymeric material was then dried overnight. Non-imprinted polymers (NIPs) were synthesized under the same conditions but without the template.

2.6. Template removal

The removal of the template was performed through acid and base hydrolysis of the template molecule. To determine the efficacy of acid and base in degrading the template protein, BSA was used as a study model. BSA samples were placed inside dialysis membranes and immersed in 6 M HCl or 4 M NaOH solutions. Dialysis was conducted for three days against HCl/NaOH and subsequently for three days against water, at two different temperatures: room temperature and 50°C. The dialysis process was halted when the pH of the dialyzed solution reached neutral, indicating the complete removal of hydrolyzing agents. After dialysis, the BSA content within the membranes was analyzed using spectrophotometry. This approach allowed for the evaluation of the hydrolysis conditions' effectiveness in removing BSA, providing an indirect indication of the protein template removal capability from the nanoparticles. In parallel, the same dialysis protocol was applied to MIP and NIP particles to assess their stability under varying pH and temperature conditions, and their integrity was evaluated using DLS.

2.7. Stability studies

Stability assessments were conducted by splitting the nanoparticles into six portions, each of which was then kept under specific conditions: controlled room temperature (25°C ± 2°C), refrigeration (5°C ± 2°C)

and freezing (-20°C ± 2°C). These conditions were tested both with and without the addition of 0.02 % (w/v) NaN_3 as a preservative [3]. Stability was also monitored for 24 hours after one day and again after 30 days post-synthesis using the Turbiscan® DNS™. Each 20 mL sample was placed in a cylindrical glass cell and maintained at 25°C within the Turbiscan. The detection head featured a pulsed near-infrared light source (880 nm) along with synchronous transmission (T) and back-scattering (BS) detectors. The T detector captured light that passed through the sample at a 180° angle from the incident beam. The detection head scanned the entire 65 mm height of the sample cell, recording T values every 40 μm, resulting in 1625 acquisitions per scan.

2.7.1. ACE2: Spike RBD (SARS-CoV-2) inhibitor screening assay

To assess the efficacy of the synthesized MIPs in inhibiting the interaction between ACE2 and the receptor-binding domain of SARS-CoV-2, an Anti-SARS-CoV-2 (BA.2) Neutralizing Antibody Titer Serologic Assay Kit was employed as per the manufacturer's guidelines.

The microplate provided in the kit was pre-coated with Human ACE2 protein, facilitating the binding of relevant components during the experiment. MIPs and NIPs samples, along with Positive and Negative Controls, were carefully added to designated wells of the microplate. Following the addition of samples, HRP-SARS-CoV-2 S protein RBD was introduced into each well, allowing for specific interactions with target molecules. The microplate was then incubated under controlled conditions, allowing for the formation of complexes between the particles and the template. Post-incubation, thorough washing of the wells was performed to remove any unbound materials, ensuring the accuracy of subsequent steps. Substrate Solution was added to each well, initiating the enzymatic reaction. This reaction was terminated by the addition of Stop Solution and the intensity of absorbance was measured at 450 nm/630 nm using a microplate reader, providing quantitative data on the interactions within the microplate. The competition between neutralizing nanoparticles in the samples and ACE2 for HRP-SARS-CoV-2 S protein RBD binding was assessed. The intensity of the assay signal decreased proportionally with the concentration of Anti-SARS-CoV-2 neutralizing synthetic antibodies.

2.7.2. Preparation of IP-QCM Sensor and Detection of protein binding via QCM

A cleaned QCM-D chip was placed in a petri dish and submerged in 4 mL of a thiol solution containing 5 mM of 16-Mercaptohexadecanoic acid (MHA) and 5 mM of 11-Mercapto-1-undecanol (MU) dissolved in a 8:2 mixture of absolute ethanol and acetic acid. This process was conducted at room temperature for 18 hours in the dark, allowing the formation of a Self-Assembled Monolayer (SAM) on the gold surface to enhance subsequent binding interactions. Following the thiol solution treatment, the chip was washed several times with absolute ethanol and dried with N_2. To activate the carboxylic groups of MHA, 100 μL of a sulfo-NHS:EDC solution (1:1, 100 mg/mL in ddH2O) was applied for 60 minutes, followed by washing with ddH2O and drying with N_2. For the immobilization of Omicron RBD domain, a standard solution was prepared at a concentration of 10 μg/mL in ddH2O. This solution was injected into the QCM-D instrument to confirm the amount of analyte bound to the sensor surface. To validate the specificity of the imprinted nanoparticles, the same immobilization procedure was applied to HSA.

The experiments, designed to investigate the binding interactions of MIP and NIP with Omicron-RBD domain, were conducted using different concentrations of the nanoparticles (12.5, 25, 50, and 100 μg/mL). The fundamental frequency was approximately 5 MHz. To establish a stable baseline, the frequency signal was calibrated by injecting ddH2O for one hour at a flow rate of 10 μL/min until the frequency signal response stabilized within ± 0.5 Hz over a ten-minute period. Following this calibration, the samples were introduced into the QCM-D instrument at the same flow rate for 50 minutes for each concentration. The QCM-D instrument recorded the frequency changes, which corresponded to the binding events between the polymers and the analyte, providing insights into the binding affinity and kinetics of these interactions. To further assess the specificity of MIP for detecting RBD domain, additional experiments were conducted where HSA was immobilized on QCM sensor chips. The binding interactions of MIP and NIP with these immobilized proteins were analysed using the same concentrations as in the initial experiments. All experiments were performed in triplicate.

2.8. Cytotoxicity test

The cytotoxicity of the nanoparticles was assessed using the MTT assay (1-(4,5-Dimethylthiazol-2-yl)-3,5-diphenyltetrazolium). BALB-3T3 cells were cultured in 48-well plates with complete media and allowed to adhere for 24 hours. Following attachment, the cells were treated with varying concentrations of both MIP and NIP nanocarriers to determine their cytotoxic effects. At the conclusion of the treatment period, 200 μl of MTT stock solution (2 mg/mL in PBS) was added to each well and incubated for 3 hours at 37°C. Post-incubation, the MTT solution was discarded, and 200 μl of DMSO was added to each well to solubilize the formazan crystals. The plate was shaken for 15 minutes, and the absorbance was measured at 570 nm using a Beckman Coulter microplate reader. Cell viability was expressed as a percentage relative to the control cells, which were considered 100 % viable. All experiments were conducted in triplicate, and the data are presented as mean values with standard deviations indicated by error bars.

2.9. Human Cell Line Activation Test (h-CLAT)

The Human Cell Line Activation Test (h-CLAT) is designed to determine the potential of substances or mixtures to induce skin sensitization through immune system activation. This assay follows the protocols set by OECD 442E and EURL ECVAM [17]. The THP-1 human leukemia monocytic cell line is used to assess the expression of co-stimulatory molecules CD54 and CD86, with nickel sulfate ($NiSO_4$) serving as a positive control. THP-1 cells were cultured in RPMI 1640 medium supplemented with 10 % FBS, 1 % Penicillin/Streptomycin, and 0.05 mM β-Mercapto-ethanol. To determine the CV75 (concentration causing 25 % mortality) in accordance with Test No. 442E: In Vitro Skin Sensitization, 1.5×10^5 cells per well were plated in a 96-well plate and incubated under standard conditions. After incubation, the cells were treated with the test substances at eight different concentrations. The next day, the treated medium was removed via centrifugation, and the cells were resuspended in FACS buffer containing propidium iodide (PI). The CV75 was calculated using flow cytometry. For the h-CLAT, 5×10^5 cells per well were plated in 24-well plates and incubated for 24 hours. Following incubation, treatments were applied, and the cells were incubated for another 24 hours. Nickel sulfate solution (100 μg/mL) and culture medium served as positive and negative controls, respectively. Post-incubation, cells were centrifuged, resuspended in FACS buffer, and divided into three aliquots. These aliquots were then treated with a blocking solution (FACS buffer containing 0.01 % γ-globulin) for 15 minutes at 4°C, followed by incubation with fluorescein-conjugated antibodies against CD86, CD54, or IgG1 (control) for 30 minutes at 4°C. After antibody incubation, cells were washed twice with FACS buffer to remove unbound antibodies, resuspended in FACS buffer containing PI, and analyzed via flow cytometry. To assess whether the test substance is a sensitizer, the Effective Concentration (EC) values for CD86 and CD54 were determined. The EC represents the concentration at which the Relative Fluorescence Intensity (RFI) equals 150 or 200, respectively. Each experiment was repeated in triplicate on three different days, and the median EC150 and EC200 values from three independent runs were reported. If only two of the three runs met the positive criteria, the higher EC150 or EC200 value was used. An increase in CD54 and CD86 expression on THP-1 cells indicates immune activation in response to a potential allergen.

3. RESULTS AND DISCUSSION

This study introduces a novel application of MIPs targeting the RBD of the SARS-CoV-2 Omicron variant S protein, presenting MIPs as a promising synthetic alternative to antibodies. Following the already tested computational protocol [21], a rational selection of an appropriate monomer for MIP selectively rebinding the Omicron variant S protein in its RBD domain has been carried out. Molecular docking combined with quantum chemical calculations was used for modeling and comparing different monomers affinity and their ability to polymerize onto the Receptor Binding Motif (RBM) portion of the S protein, thus preventing its binding to ACE2 receptor.

The used approach has foundation on the considerable amount of different functional groups present in the target protein that creates potential premises for multiple noncovalent interactions (H-bond, van der Waals, electrostatic, and/or hydrophobic) between the protein and functional monomers in a pre-polymerization complex before protein-MIP synthesis. It can be assumed that these interactions can orient the polymerization process and play a crucial role in the formation of complementary binding sites after the template protein removal, that is necessary for the subsequent selective rebinding of the target protein to the MIP. On this basis, the evaluation of all possible noncovalent interactions binding sites as well as their strength in the protein-monomer complex must be taken into account for the aim to design MIPs targeting specific proteins with highly selective recognition sites. Here, the aim is to compare, using a molecular modeling approach, the different capability of different functional monomer for building a polymer with macromolecular imprints capable of selectively rebind protein-sized analytes.

Molecular docking was applied to find both energetically favorable binding poses of the selected functional monomer on the model protein and to predict the probable arrangement of multiple monomer molecules around the macromolecular target. A particular attention has been put in partial charges calculation on the functional monomers since the small dimension of the molecules considered (AAm, AAc/acrylate, NIPAM, nPMA, TBAm), will allow them to easily binds on the protein target surface, and the electron density and charge distribution are primary responsible of the electrostatic/hydrophobic noncovalent complex stabilization.

The approach was based on using the docking of each of the monomers throughout all the RBD surface to determine the energetically favorable binding poses and finally to assess the cumulative strength of H-bond interactions between the monomers and the sterically accessible proton-acceptor groups of RBD, such as polar amino acid. The most populated clusters for all the considered monomers are highlighted in Table 1.

3.1. Acrylic acid docking results

The results obtained from the docking of AAc identified a close cluster distribution. We excluded those poses that are not accessible to the SAS (Solvent Accessible Surface) surface or that lie at the interface between monomers in the trimeric S protein association (pdb code 6vsb), and we observe that among the selected clusters two zones are covered, being one on the center of the RBM portion of the RBD domain. As can be seen in Fig. 1, they are distributed with cluster population of Cl1 (7 %) far from RBM, Cl2 (12 %) RBM), Cl3 57 % lateral, Cl4 24 % near Cl3. This spread distribution, together with a comparable population percentage, and comparable binding energy suggest that this monomer can efficiently binds and include the RBM portion of the target protein occupying positions that can efficiently lead to the desired polymerization process.

3.1.1. Acrylamide docking results

The results obtained from the docking of AAm showed the existence of several accessible clusters but with high different populations spread all over the RBD surface. The most populated cluster (29 %) is located within the RBM-6 residues portion. The other four clusters are dispersed around the RBD, but they are not near the six key residues; instead, they are situated in the outer region relative to the contact surface (Fig. 2). More, the Cl4 has 16 % pop and Cl5 18 %. The populated distribution of these clusters together with the highest population of the binding pose in the RBM, suggest that AAm is highly suitable to be considered as a promising monomer for targeted polymerization (Fig. 3).

Building on the previous results, an emulsion polymerization reaction was employed to synthesize imprinted nanoparticles with high specificity and functionality using AAm and AAc as functional monomers. Emulsion polymerization offers numerous advantages, including high yield and good reproducibility. Additionally, this method is particularly suitable for protein imprinting due to its ability to produce nanoparticles with specific binding sites for target molecules. MIPs obtained through this process exhibit significant potential in various applications, such as controlled drug release, protein purification, and the development of highly specific sensors [9]. In this work, a water-in-oil emulsion system was utilized, where the aqueous phase contained the monomers, cross-linking agents, and template molecules. These components were meticulously dispersed into the oil phase, which consisted of an immiscible solvent. The role of surfactants was paramount in this setup, as they facilitated the formation of a stable emulsion by reducing the interfacial tension between the aqueous and oil phases. The injection system setup was crucial for forming a stable emulsion and achieving nanosized particles. The fine gauge of the 30 G stainless steel needle allowed for precise control over the injection of the water phase into the oil phase, promoting the formation of uniform spherical droplets. Coupled with the syringe pump's ability to regulate flow rates meticulously, this setup ensured consistent droplet size and distribution, which are essential for producing nanosized particles with high stability. This approach not only enhanced the reproducibility of the emulsion but also optimized the overall efficiency of the polymerization process. The careful selection of monomers and cross-linking agents, combined with the optimized emulsion conditions, was crucial in achieving nanoparticles with the desired physical and chemical properties. The obtained nanoparticles were analyzed in terms of size, polydispersity index (PdI), and ζ-potential using DLS. The results for MIPs and NIPs are shown in Table 2 and Fig. 4:

The MIP nanoparticles exhibited an average size of 40.24 ± 6.383 nm, while the NIP nanoparticles had a slightly smaller average size of 35.95 ± 5.467 nm. Although the difference in average sizes is not substantial, it suggests that MIPs tend to be slightly larger than NIPs, likely due to varying interactions between monomers and the template.

Table 1
Most populated clusters for the considered monomers in kJ/mol. "Close/Near RBM" clusters are highlighted in red, while "Far from RBM" clusters are highlighted in blue.

Cluster n.	AAm	Cluster n.	AAc	Cluster n.	NiPAM	Cluster n.	nPMA	Cluster n.	TIBAm
Cl1 (29 %)	−14.5	Cl1 (7 %)	−16.6	Cl1 (88 %)	−18.8	Cl1(15 %)	−22.3	Cl1 (78 %)	−20.10
Cl2 (5 %)	−14.2	Cl2 (12 %)	−.16.0	Cl2 (6 %)	−17.0	Cl2 (18 %)	−21.8	Cl2-Cl3 (25 %)	−19.1
Cl3 (2 %)	−14.1	Cl3 (57 %)	−15.8			Cl3-Cl6 (15 %)	−20.9/−19.1	Cl4 (8 %)	−17.7
Cl4(16 %)	−14.0	Cl4 (24 %)	−15.7			Cl7(37 %)	−19.0	Cl5 (9 %)	−15.9
Cl5(18 %)	−13.9								

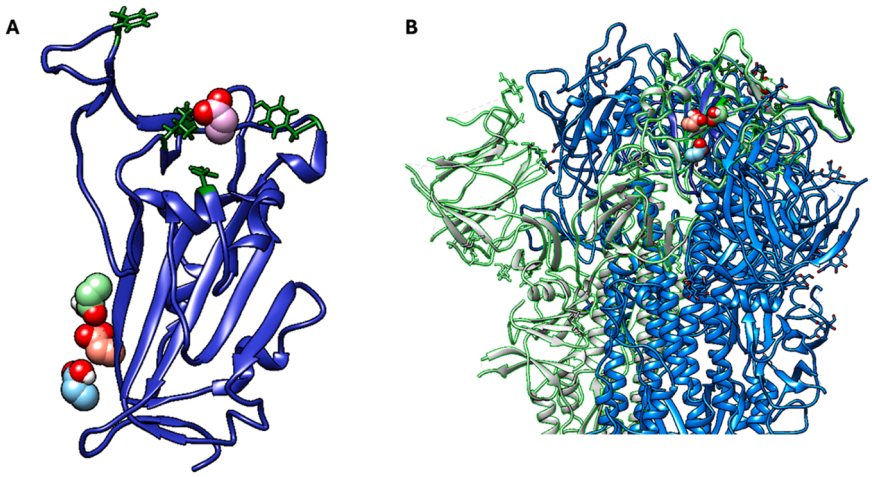

Fig. 1. AAc clusters distributions accessible to solvent surface on RBD domain of S protein (8uir). (A) In forest green are highlighted the 6 key residues implicated in ACE2 binding (resuled 417,455, 486 493,494, 501). (B) Superimpostion of RBD 7yow with docked clusters for AAm and 8uir.

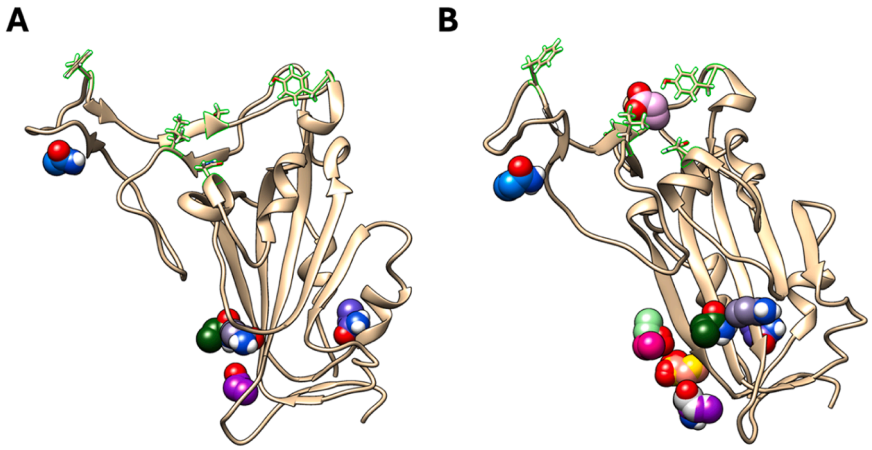

Fig. 2. (A) AAm clusters (spheres) distributions accessible to solvent surface on RBD domain of S protein (gold ribbons). In green are highlighted the 6 key residues implicated in ACE2 binding (resuled 417,455, 486 493,494, 501). (B) AAm clusters together with AAc ones (CPK spheres, RBD in ribbons).

Both MIP and NIP nanoparticles had a PdI of less than 0.3, indicating a relatively narrow size distribution and good size uniformity. In number, the main population of NPs have instead a mean diameter of 124 nm, whereas the peak centered at 60 nm accounts for less than 4 % of the total number of particles (5.98 $\times$10 8 $\pm$7.6$\times$10 7 particles/mL). NTA analysis also highlighted a small percentage (about 3.7 %) of nanoparticles having a mean diameter of 200 nm (Fig. 5).

Additionally, the ζ-potential measurements for both MIP and NIP nanoparticles were negative and of similar magnitude, indicating that both types of nanoparticles are stable in suspension due to sufficient electrostatic repulsion, which prevents aggregation (Table 2). To confirm the consistency of the data, TEM images were used to determine the particle size of MIPs (Fig. 6). The analysis showed that the particles had a spherical shape and sizes comparable to those obtained from DLS measurements.

In summary, the results indicate that MIP and NIP nanoparticles have comparable sizes and stability. MIP nanoparticles are slightly larger with a narrower size distribution compared to NIP nanoparticles. The high stability of the nanoparticles, evidenced by ζ-potential values, confirms their suitability for various applications.

Template removal is a crucial step for the optimal performance of MIPs, ensuring no template molecule residues occupy the active sites within the particle structure, making them available for rebinding the target molecule [8]. Various methods can be used for removal, including protein hydrolysis, which was employed in this work. This method was chosen because the template molecule, in this case, is a protein too large to pass through a common dialysis membrane. Therefore, the protein must first be hydrolyzed into smaller fragments, which can then be dialyzed and removed from the imprinted polymer.

After completing the BSA tests and defining optimal hydrolysis conditions (Fig. 2S), alkaline hydrolysis was performed on particles imprinted with the SARS-CoV-2 RBD and their corresponding NIP (Fig. 3S). Dialysis waters were lyophilized, concentrated, and analyzed for RBD presence via spectroscopy, indicating a template removal efficiency of 96 $\pm$ 2.6 %. These overall results indicate that alkaline hydrolysis at 50°C is the optimal combination for ensuring both effective template removal and polymer stability. After complete dialysis, the final particles suspension concentrations, based on lyophilized masses, were approximately 14.68 mg/mL for MIP and 9.64 mg/mL for NIP, corresponding to yields of about 82.98 % and 78.21 %, respectively.

Nanomedicines will not achieve success as pharmaceutical products until they undergo comprehensive evaluation of various quality aspects, particularly pharmaceutical stability during storage. Stability testing is essential in drug development to assess how a product's quality changes over time under environmental factors like temperature, humidity, and light. This testing helps establish the drug's shelf life and recommend suitable storage conditions [20]. Stability tests over time were performed in the presence or absence of sodium azide as a preservative,

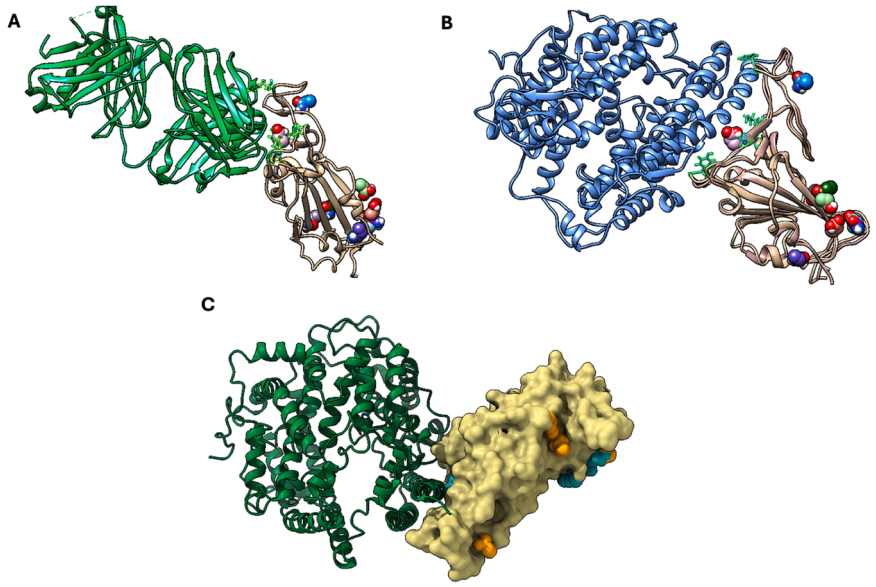

Fig. 3. (A) AAm and AAc clusters (CPK spheres) distributions accessible to solvent surface on RBD domain of S protein (gold ribbons) in complex with NCV2SG48 Fab (watergreen ribbons) (7yow). In green are highlighted the 6 key residues implicated in ACE2 binding (resuled 417,455, 486 493,494, 501). (B) Aam and AAc clusters (CPK spheres) distributions accessible to solvent surface on RBD domain of S protein (gold ribbons) in complex with ACE2 receptor (blue ribbons) (7c8d). In green are highlighted the 6 key residues implicated in ACE2 binding (resuled 417,455, 486 493,494, 501). (C) Same as B but RBD is shown with its molecular surface; AAm in yellow CPK, AAc in cyan CPK. Following the established protocol detailed in the methods section, molecular docking studies have been conducted on additional monomers (NIPAM, nPMA and TBAm) to assess the potential suitability of these compounds as monomers for polymers synthesis (Fig. 1S). The outcomes of these docking calculations indicated that these monomers are not adequate for polymer imprinting, and the detailed results are described in the supplementary information.

Table 2
Z-Average size, PdI and ζ-Potential Data for MIPs and NIPs.

	Z-Average	PdI	ζ-potential (mV)
MIP	40.24 ± 6.383	0.183	−33.3 ± 8.14
NIP	35.95 ± 5.467	0.213	−34.2 ± 5.89

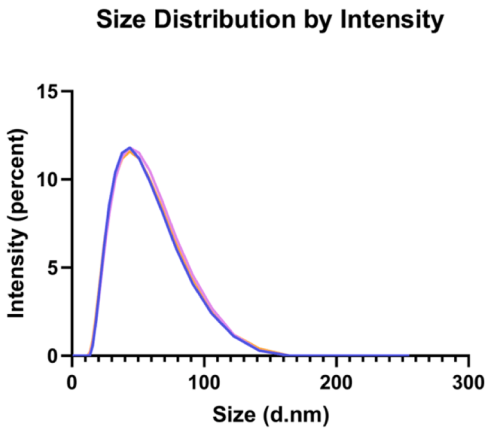

Fig. 4. Hydrodynamic diameter of MIP particles measured by DLS.

under different temperature conditions [3]. Sodium azide was chosen for its common use in antibody preservation, preventing microbial contamination. The goal was to evaluate variations in dimensional parameters, such as size, PdI, and ζ-potential, under different storage conditions. A PdI value up to 0.3 indicates a relatively narrow size distribution and particles with ζ-potential values of ± 30 mV are considered highly stable. Results after 24 hours and after 30 days are shown in Figs. 4S and 5S, respectively. Results after 24 hours indicate that samples stored at 25°C with NaN_3 show an increase in size and PdI compared

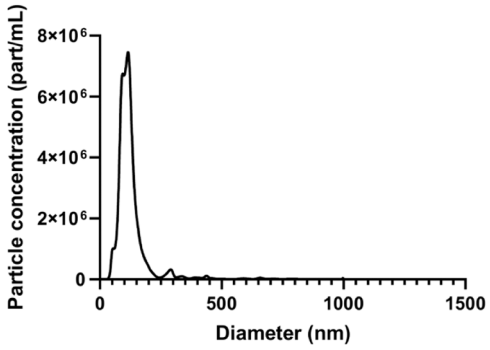

Fig. 5. Exemplification of the NTA pattern of MIP.

to samples stored without NaN_3 at the same temperature, while ζ-potential slightly decreases (Figure 4SA). Samples stored at 4°C with NaN_3 show a slight difference in both size and PdI, and a significant decrease in ζ-potential compared to those stored without the preservative (Figure 4SB). Finally, samples stored at −20°C with NaN_3 show no significant variations in examined parameters (Figure 4SC). These results indicate that NaN_3 presence can influence the dimensional stability and ζ-potential of nanoparticles, with variations depending on storage temperature. Storage at room temperature with NaN_3 leads to an increase in size and PdI, suggesting possible interactions between the preservative and nanoparticles. Conversely, storage at lower temperatures (4°C and −20°C) seems to mitigate these effects, maintaining the nanoparticles' properties more stable over time.

After 30 days of storage at 25°C, the addition of the preservative has a consistently negative effect on all three parameters, as illustrated in Fig. 5S. Similar detrimental effects are observed during storage at 4°C. At −20°C storage, the presence of NaN_3 results in a slight increase in both size and PdI, while the ζ-potential remains stable. Based on the data obtained, it can be concluded that the developed synthetic antibody in

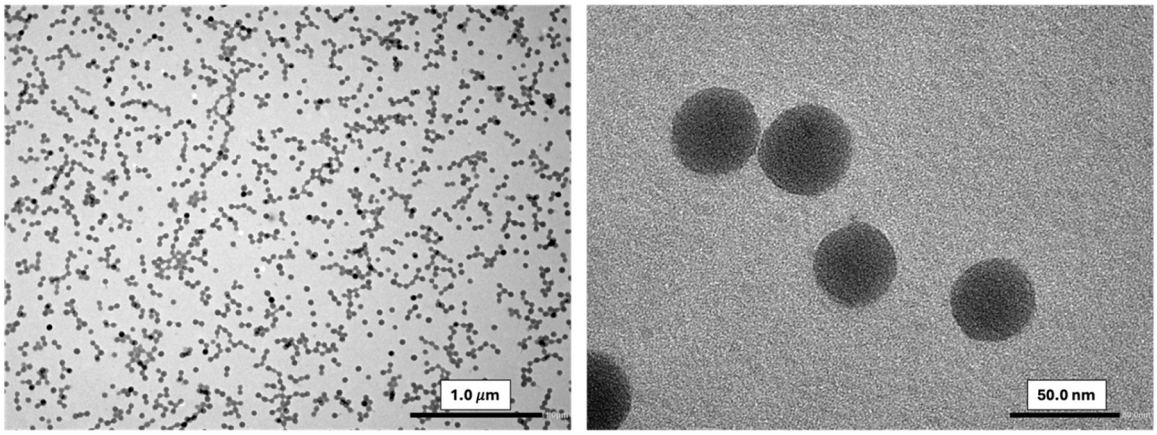

Fig. 6. TEM Micrographs of MIP particles.

this study demonstrates exceptional stability at room temperature, highlighting its practicality for routine use and storage. The observed dimensional changes over the evaluation period were minimal and statistically insignificant. Moreover, the most favorable results were achieved in the absence of a sodium azide. This characteristic presents a significant advantage over biological antibodies, which necessitate stringent storage conditions, including specific temperatures and the maintenance of a cold chain during transport, as well as the addition of preservatives. Therefore, the synthetic antibody could be a more viable option for various applications where stability and ease of storage are critical.

The stability of nanoparticles suspensions, prepared in both distilled water and PBS at pH 7.4 (10^{-3} M), was further evaluated using a Turbiscan® DNS™. This technique measures changes in the intensity of light transmitted (ΔT%) and backscattered (ΔBS%) by the sample. These measurements are then converted into a global stability kinetics value, represented by the Turbiscan Stability Index (TSI) [5]. Figs. 6S and 7S illustrate the changes in ΔT% and ΔBS% as a function of sample height and time in the suspensions, analyzed at both one day and 30 days post-synthesis. The data reveal that the samples maintained their stability over the observed periods, with variations in both parameters consistently within a 10 % range throughout the 24-hour analysis. The positive variation in ΔT% at the top of the samples, observed consistently at both time points, indicates a creaming phenomenon, which was reversible upon slight agitation. In the midsection of the samples, both backscattering and transmission measurements remained stable, indicating no significant particle aggregation or size variation. These findings suggest that the observed destabilization is primarily due to the migration of particles, rather than changes in particle size, and that the colloidal stability of the suspensions is preserved even after 30 days.

Moreover, the TSI, a destabilization factor calculated by summing changes in ΔT% or ΔBS% of the light in successive measurements as a function of sample height, remained low (TSI < 0.9), confirming the stability of the imprinted nanoparticles in both water and PBS (Table 3).

The stability assessments conducted in this study reinforce the practical viability of MIPs in field and clinical settings. Unlike natural antibodies, MIPs displayed minimal degradation or aggregation over 30 days, maintaining their structural and colloidal integrity, even at room temperature. This stability under ambient conditions could be particularly valuable in low-resource settings, where cold-chain logistics are challenging or impractical. By offering a reliable and durable alternative to biological reagents, MIPs could become central to diagnostic kits and therapeutic formulations.

Once the MIPs were synthesized, their ability to inhibit the interaction between the ACE2 receptor and the SARS-CoV-2 RBD (BA.2) was

Table 3
Turbiscan Stability Index (TSI) of imprinted particles in distilled water and PBS at various time intervals, measured one day and 30 days post-synthesis. Results are presented as means ± standard deviation (n = 3).

	Analysis after one day				Analysis after 30 days			
	4 h	8 h	12 h	24 h	4 h	8 h	12 h	24 h
H_2O	0.14 ± 0.09	0.15 ± 0.11	0.16 ± 0.14	0.28 ± 0.13	0.32 ± 0.10	0.44 ± 0.09	0.51 ± 0.12	0.60 ± 0.14
PBS	0.52 ± 0.08	0.62 ± 0.011	0.65 ± 0.14	0.76 ± 0.11	0.45 ± 0.07	0.55 ± 0.12	0.58 ± 0.15	0.81 ± 0.06

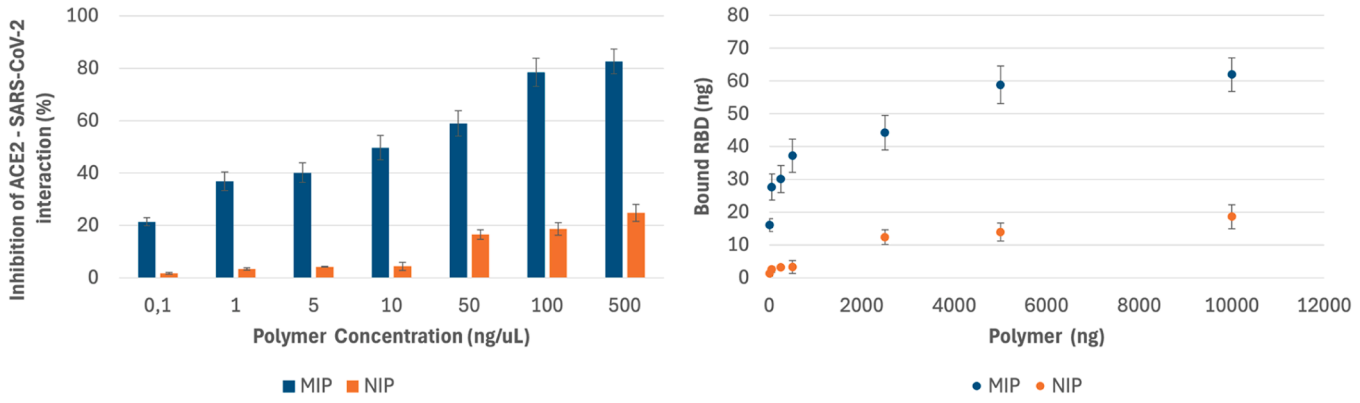

Fig. 7. Inhibitor Screening Assay: (A) Inhibition of ACE2-SARS-CoV-2 RBD interactions and (B) binding isotherms of 1,5 μg/mL SARS-CoV-2 RBD to imprinted and non-imprinted nanoparticles.

evaluated using a neutralizing anti-SARS-CoV-2 antibody assay kit. Data were obtained by measuring the absorbance intensity at 450 nm/630 nm using a microplate reader. Specifically, the competition between the neutralizing nanoparticles in the sample and ACE2 for binding to the horseradish peroxidase-conjugated SARS-CoV-2 S protein RBD molecules was assessed. Imprinted and non-imprinted nanoparticles were tested at different concentrations ranging from 0.1 ng/μL to 500 ng/μL. The obtained results (Fig. 7A) confirmed the ability of the developed system to reduce RBD binding to the ACE2 receptor in a concentration-dependent manner. In fact, the graph shows that for the MIP, as the polymer concentration increases, the inhibition percentage also increases; this is expected as the imprinted polymer contains cavities necessary to interact with the SARS-CoV-2 RBD, thus preventing its interaction with the ACE2 receptor. Conversely, the NIPs did not exhibit significant inhibition of the RBD-ACE2 interaction. The absence of specific binding cavities in the NIPs, which are crucial for binding the template molecule, accounts for this lack of inhibition. The minor inhibition observed with the NIPs is likely due to non-specific interactions with the target molecule.

Furthermore, the collected data were used to calculate the amount of SARS-CoV-2 RBD bound to the polymers (MIP and NIP). The results are shown in Fig. 7B and confirm that MIPs are capable of binding a greater amount of the template molecule compared to the corresponding non-imprinted particles.

The mechanism by which MIPs inhibit RBD-ACE2 binding suggests that the synthetic polymer matrix successfully mimics the binding characteristics of natural antibodies, a significant achievement in the field of molecular imprinting. The imprinted cavities in MIPs provide a highly selective environment that aligns with the spatial and chemical properties of the RBD, enabling strong and specific interactions. These cavities create a template-like effect that physically blocks the RBD from engaging with the ACE2 receptor, a critical step in viral entry. This selective inhibition, observed through this competitive binding assays, demonstrates that MIPs can effectively reduce viral infectivity by impeding the initial stages of the virus-host interaction.

To further highlight the functionality of MIP particles, comprehensive binding studies were performed using a QCM-D instrument. The process began with the functionalization of the sensor surface using a SAM composed of a mixture of MHA and MU, which act as spacers to enhance the interaction between the gold coating and the analyte. MHA was then attached using sulfo-NHS:EDC coupling chemistry. Changes in resonant frequency, shown in Fig. 8, were used to monitor the binding progression.

Using the Sauerbrey equation [26], the quantities of analytes on the sensor surface were determined, revealing an RBD density of 8.19 $\times 10^{-13}$ mol/cm^2 and an HSA density of 8.43 $\times 10^{-13}$ mol/cm^2. These functionalized QCM chips were then used to evaluate the binding interactions of MIP and NIP with analyte and control. The introduction of varying concentrations of nanoparticles results in a concentration-dependent frequency change, as depicted in Fig. 9.

The highest resonant frequency changes were observed (Fig. 9A), indicating strong affinity of MIP for Omicron-RBD at low concentrations. As the concentration of MIP increased, the affinity remained stable, reaching saturation after 180 minutes of injection. The introduction of the MIPs resulted in significant decreases in frequency compared to the injection of dispersions containing NIP that have the same chemical composition. This observation underscores the importance of the MIPs cavities in facilitating the recognition of the template molecules. These imprinted cavities are more effective in distinguishing and binding to the target molecules than the non-specific intermolecular interactions that occur on the surface of the nanogel [15]. A different result was observed when MIPs and NIPs were injected onto QCM-D sensors functionalized with HSA, as shown in Fig. 9B. The affinity for HSA was notably low for both MIPs and NIPs, which underscores the high specificity and effectiveness of the selected imprinting technology in distinguishing between different proteins. As depicted in Fig. 10, this result demonstrates that the imprinting technique is highly selective, ensuring that the MIPs are specifically tailored to recognize and bind to their target molecules rather than interacting with non-target proteins like HSA.

Apparent dissociation constants (K_D) were derived by fitting the Langmuir isotherm to the experimental data collected from the QCM frequency shift measurements (Table 4) [6].

These results serve to emphasize and elucidate the considerable promise and effectiveness of MIP particles as a versatile and potent tool for specifically recognizing RBD, compared to NIP, where MIPs demonstrate a higher degree of selectivity towards RBD with an approximative K_D of 9.5. A higher K_D was observed for HSA, while R^2 was lower than RBD R^2 value. This observation underscores the unique capacity of MIPs for precise molecular recognition. Furthermore, MIP exhibit a robust and tailored recognition capability for template, suggesting their substantial potential and applicability in the treatment and prevention of SARS-CoV-2 infection.

Safety evaluations were conducted to assess potential cytotoxicity and immunogenicity of the test substances. These evaluations employed two established in vitro methods: the MTT assay and the human Cell Line Activation Test (h-CLAT).

The MTT assay offers a quick and economical approach to evaluate cell proliferation. This technique hinges on the conversion of the yellow tetrazolium compound into violet/black insoluble formazan crystals by living cells. Results from MTT assays performed on Balb/3T3 cells, following treatment with escalating concentrations of nanoparticles, showed no notable reduction in cell viability (Fig. 11). The nanocarriers exhibited no toxicity to viable cells, demonstrating their biocompatibility.

Moreover, to determine the sensitizing potential of MIP and NIP, the

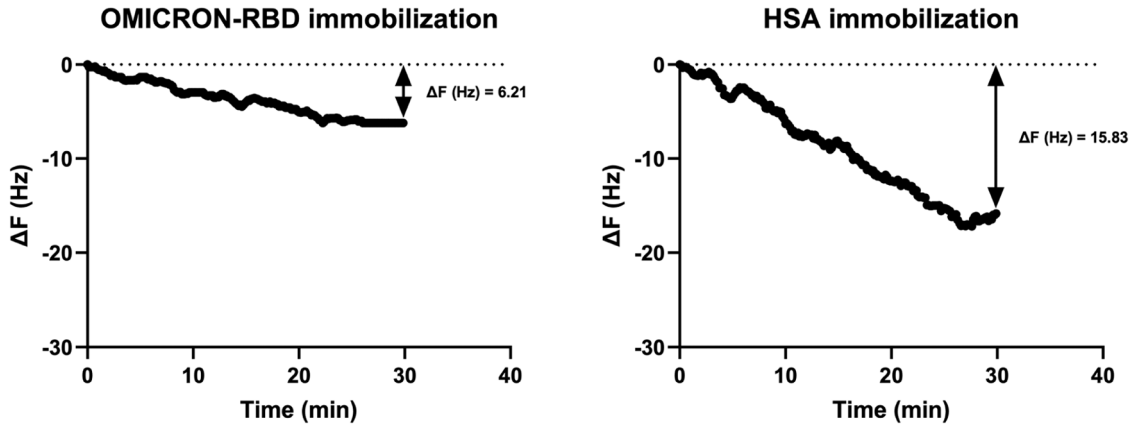

Fig. 8. Analyses of QCM-D sensor modification with RBD domain of Omicron variant and HSA.

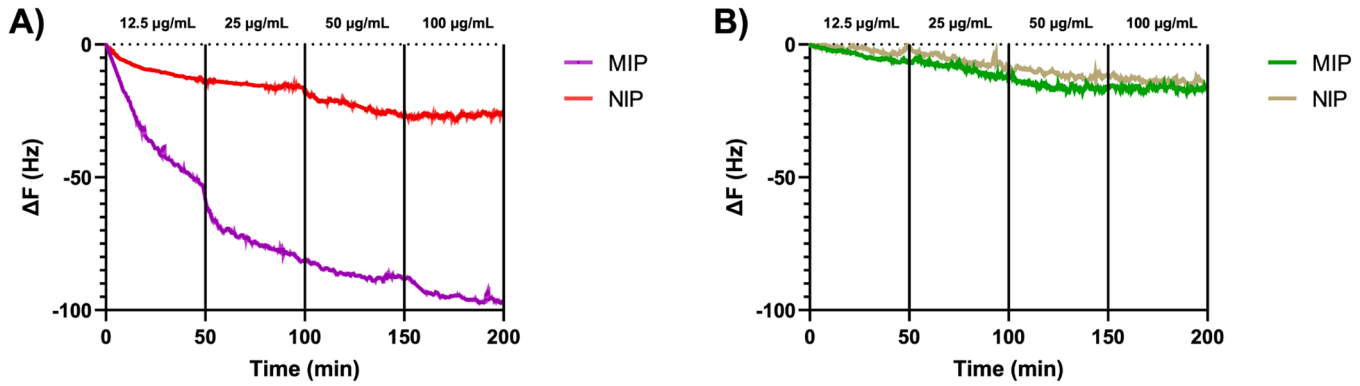

Fig. 9. Real-time changes in resonant frequency (ΔF) after repeated injections of increasing concentrations of MIP and NIP dispersions on functionalized QCM-D sensor chips with (A) RBD and (B) HSA.

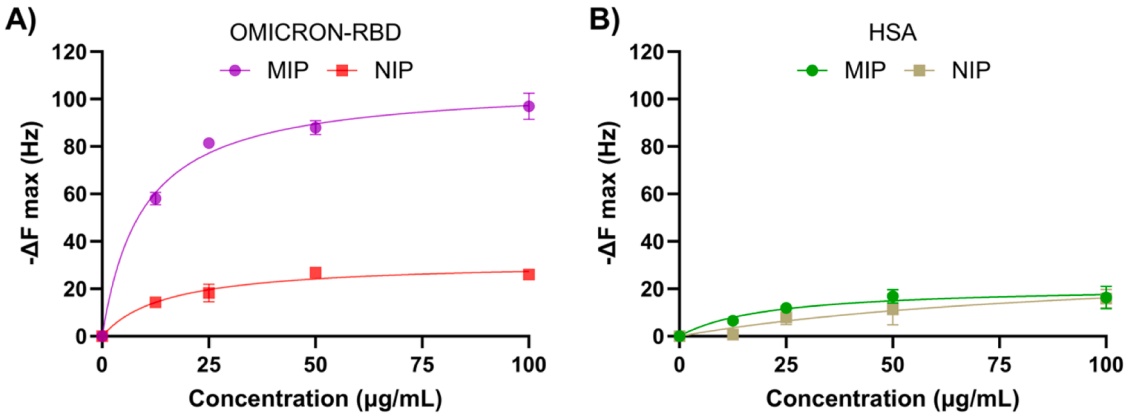

Fig. 10. Binding isotherms of MIP and NIP on OMICRON-RBD (A) and HSA (B) functionalized sensor chip.

Table 4
Equilibrium dissociation constant (K_D) of MIP and NIP.

	Omicron-RBD		HSA	
	K_D	R^2	K_D	R^2
MIP	9.5±5.4	0.99	21.0±14.3	0.96
NIP	15.0±8.7	0.97	22.3±15.8	0.94

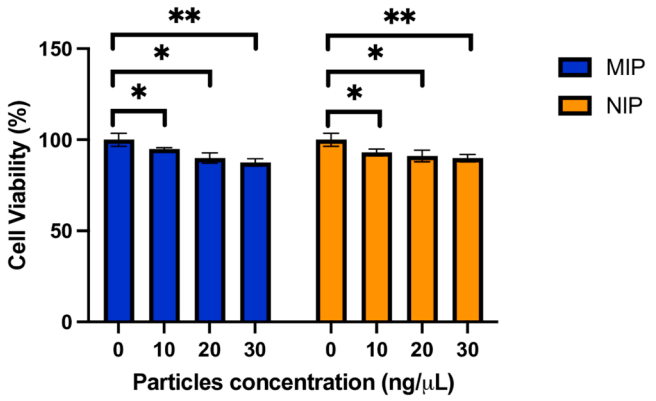

Fig. 11. Cell viability: the MTT test was conducted on Balb/3T3 cells following a 24-hour exposure to escalating concentrations of MIP and NIP. Data are expressed as means ± SEM, statistical significance: *p < 0.05, **p < 0.01.

h-CLAT was conducted following the guidelines of OECD 442E. This assay measures the expression levels of CD86 and CD54 markers in THP-1 cells. These levels are assessed based on their activation capacity using flow cytometry after a 24-hour exposure to eight serial concentrations of the test substances. The concentrations used are derived from a preliminary cytotoxicity study that identifies the CV75 of the compound on the cells.

The sensitization potential of the test items was evaluated using the Relative Fluorescence Intensity (RFI%) values for CD86 and CD54. A substance is predicted to be a sensitizer if the RFI% value for CD86 is ≥150 % and/or the RFI% value for CD54 is ≥200 % in at least two independent runs. Conversely, a negative prediction for sensitization is made if the RFI% value for CD86 is <150 % and/or the RFI% value for CD54 is <200 %.

The results, presented in Table 5, indicate that the tested samples did not exhibit skin sensitizing properties, affirming the overall safety and biocompatibility of the nanoparticles.

In summary, the adaptability of MIPs makes them a versatile platform for managing infectious diseases, especially zoonotic diseases with high mutation rates. In this study, the methodology used to imprint SARS-CoV-2 RBD can be applied to other pathogens, suggesting that

Table 5
RFI% value of CD54 and CD86 on THP-1 monocytes.

SAMPLES	CD54	CD86
MIP	141	121
NIP	133	119
NEGATIVE CONTROL	110	101
POSITIVE CONTROL	301	277
CUT-OFF	200	150

MIPs could serve as a foundational technology in pandemic preparedness. By altering the imprinting process to reflect different viral proteins or epitopes, MIPs can be readily adapted to recognize new targets, providing a rapid-response solution that could accelerate diagnostics and therapeutic interventions in future outbreaks.

4. Conclusion

The development of MIPs as synthetic antibody alternatives represents a significant advancement in the fight against rapidly evolving pathogens, like SARS-CoV-2. This study focused on engineering MIPs to selectively bind the RBD of the Omicron variant S protein, demonstrating that MIPs can serve as both diagnostic and potential therapeutic tools in controlling viral spread.

Stability assessments demonstrated that these MIPs remained well-dispersed and stable under various conditions, including room temperature, refrigeration, and freezing, over a 30-day period. The stability was consistently confirmed by stable TSI values, indicating that the MIPs preserved their functional properties throughout this time frame and emphasizing their suitability for long-term storage and scalability. MIPs exhibited significantly higher binding efficacy compared to NIPs, due to the specific imprinting of the RBD during their synthesis. This process endowed the MIPs with enhanced binding capabilities, whereas NIPs lacked these specific binding sites, leading to much lower affinity for the RBD. Additionally, MIPs demonstrated a concentration-dependent inhibition of the interaction between the ACE2 receptor and the RBD, with higher concentrations resulting in greater inhibition. Quantitative analysis of binding affinity demonstrated that MIPs achieved an apparent dissociation constant of 9.5 for the RBD, showcasing a strong and specific interaction with the target protein, which contrasts markedly with the limited binding efficacy of NIPs. The QCM-D studies underscored the MIPs significant potential for precise molecular recognition and application in SARS-CoV-2 detection and treatment, compared to NIPs and non-target proteins like HAS.

Further tests confirmed the biocompatibility of MIPs, as shown by the MTT assay on Balb/3T3 cells, which indicated that neither MIPs nor NIPs were significantly cytotoxic, suggesting their potential for therapeutic applications. The h-CLAT also indicated no sensitizing potential, thus supporting the MIPs' safety for biomedical applications. Further studies should evaluate their performance in biological systems, specifically their pharmacokinetics, biodistribution, and potential for immune system activation. Moreover, conducting in vivo studies with animal models could provide critical data on MIPs' safety and efficacy, paving the way for clinical trials.

Overall, the findings highlight MIPs as a promising platform for creating synthetic antibodies with high specificity, efficacy, and stability. Unlike traditional biological antibodies, which may struggle with effectiveness, stability, and production speed as new virus variants emerge, MIPs offer significant advantages. Their flexibility and adaptability allow for rapid design and production, making them a valuable tool in addressing novel viral threats. The demonstrated stability and biocompatibility of MIPs further enhance their practical utility, positioning them as a reliable alternative to conventional antibodies in the ongoing fight against COVID-19 and future viral outbreaks.

Author contributions: CRediT

Conceptualization, M. D., O. I. P. and F. P. (Francesco Puoci); methodology, M. D., F. P. (Francesco Patitucci), O. I. P., M. F. M., S. F., I. P., R. G.; validation, S. P. and M. C.; formal analysis, M. D., S. P.; investigation, M. D., M. C., F. P. (Francesco Patitucci), and S. P.; data curation, M. D., S. F. and O. I. P.; writing – original draft, M. D., O. I. P., F. P. (Francesco Patitucci), S. F., R. G. and M. F. M.; writing – review and editing, O. I. P.; supervision, M. D., O. I. P. and F. P. (Francesco Puoci); project administration, O. I. P. and F. P. (Francesco Puoci); funding acquisition, F. P. (Francesco Puoci). All authors have read and agreed to the published version of the manuscript.

CRediT authorship contribution statement

Silvia Franzè: Writing – original draft, Methodology, Data curation. **Ida Perrotta:** Methodology. **Sabrina Prete:** Validation, Formal analysis. **Roberta Galeazzi:** Writing – original draft, Methodology. **Mariangela Caravelli:** Validation, Investigation. **Ortensia Ilaria Parisi:** Writing – review & editing, Writing – original draft, Supervision, Project administration, Methodology, Data curation, Conceptualization. **Francesco Puoci:** Supervision, Project administration, Funding acquisition, Conceptualization. **Francesco Patitucci:** Writing – original draft, Methodology, Investigation. **Marisa Motta:** Writing – original draft, Methodology. **Marco Dattilo:** Writing – original draft, Supervision, Methodology, Investigation, Formal analysis, Data curation, Conceptualization.

Declaration of Competing Interest

The authors declare that they have no known competing financial interests or personal relationships that could have appeared to influence the work reported in this paper

Acknowledgements

M. D. was funded by the National Plan for NRRP Complementary Investments (PNC, established with the decree-law 6 May 2021, n. 59, converted by law n. 101 of 2021) in the call for the funding of Research Initiatives for Technologies and Innovative Trajectories in the Health and Care Sectors (Directorial Decree n. 931 of 6 June 2022)—project n. PNC0000003—AdvaNced Technologies for Human-centrEd Medicine (project acronym: ANTHEM). This work reflects only the authors' views and opinions, and neither the Ministry for University and Research nor the European Commission can be considered responsible for them. O. I. P. and F. P. (Francesco Patitucci) were funded by PON "Ricerca e Innovazione'' 2014–2020, Asse IV "Istruzione e ricerca per il recupero'', Azione IV.4—"Dottorati e contratti di ricerca su tematiche dell'innovazione''.

Appendix A. Supporting information

Supplementary data associated with this article can be found in the online version at doi:10.1016/j.colsurfb.2024.114408.

Data availability

Data will be made available on request.

References

[1] A. Bajaj, J. Trimpert, I. Abdulhalim, Z. Altintas, Synthesis of molecularly imprinted polymer nanoparticles for SARS-CoV-2 virus detection using surface plasmon resonance, Chemosensors 10 (2022) 459.
[2] T.S. Bedwell, M.J. Whitcombe, Analytical applications of MIPs in diagnostic assays: future perspectives, Anal. Bioanal. Chem. 408 (2016) 1735–1751.
[3] C. Contardi, D. Rubes, M. Serra, R. Dorati, M. Dattilo, L. Mavliutova, M. Patrini, R. Guglielmann, Br Sellergren, E. De Lorenzi, Affinity Capillary Electrophoresis as a Tool To Characterize Molecularly Imprinted Nanogels in Solution, Anal. Chem. 96 (2024) 3017–3024.
[4] M. Dattilo, M.F. Motta, F. Patitucci, C. Ferraro, O.I. Parisi, F. Puoci, Exploring Crosslinker Effects on Fluorescent Molecularly Imprinted Polymers for Improved Gefitinib Delivery in Lung Cancer Theranostics, Mater. Adv. (2024).
[5] R.M. Derbali, V. Aoun, G. Moussa, G. Frei, S.F. Tehrani, J.C. Del'Orto, P. Hildgen, V.G. Roullin, J.L. Chain, Tailored nanocarriers for the pulmonary delivery of levofloxacin against Pseudomonas aeruginosa: a comparative study, Mol. Pharm. 16 (2019) 1906–1916.
[6] E.A. Dubiel, B. Martin, S. Vigier, P. Vermette, Real-time label-free detection and kinetic analysis of Etanercept—Protein A interactions using quartz crystal microbalance, Colloids Surf. B: Biointerfaces 149 (2017) 312–321.
[7] J. García-Calzón, M. Díaz-García, Characterization of binding sites in molecularly imprinted polymers, Sens. Actuators B: Chem. 123 (2007) 1180–1194.

[8] M. Garg, N. Pamme, Strategies to remove templates from molecularly imprinted polymer (MIP) for biosensors, TrAC Trends Anal. Chem. (2023) 117437.
[9] K. Haupt, P.X. Medina Rangel, B.T.S. Bui, Molecularly imprinted polymers: Antibody mimics for bioimaging and therapy, Chem. Rev. 120 (2020) 9554–9582.
[10] C. Herrera León, N.A. Kalacas, A. Mier, P. Sakhaii, F. Merlier, E. Prost, I. Maffucci, V. Montagna, H. Mora-Radó, P.K. Dhal, Synthetic Peptide Antibodies as TNF-α Inhibitors: Molecularly Imprinted Polymer Nanogels Neutralize the Inflammatory Activity of TNF-α in THP-1 Derived Macrophages, Angew. Chem. 135 (2023) e202306274.
[11] C.B. Jackson, M. Farzan, B. Chen, H. Choe, Mechanisms of SARS-CoV-2 entry into cells, Nat. Rev. Mol. Cell Biol. 23 (2022) 3–20.
[12] J. Jiang, G. Oberdörster, P. Biswas, Characterization of size, surface charge, and agglomeration state of nanoparticle dispersions for toxicological studies, J. Nanopart. Res. 11 (2009) 77–89.
[13] R. Khandia, S. Singhal, T. Alqahtani, M.A. Kamal, A. Nahed, F. Nainu, P.A. Desingu, K. Dhama, Emergence of SARS-CoV-2 Omicron (B. 1.1. 529) variant, salient features, high global health concerns and strategies to counter it amid ongoing COVID-19 pandemic, Environ. Res. 209 (2022) 112816.
[14] N.D. Kushwaha, J. Mohan, B. Kushwaha, T. Ghazi, J.C. Nwabuife, N. Koorbanally, A.A. Chuturgoon, A comprehensive review on the global efforts on vaccines and repurposed drugs for combating COVID-19, Eur. J. Med. Chem. (2023) 115719.
[15] A. Lamaoui, A.A. Lahcen, A. Amine, Unlocking the Potential of Molecularly Imprinted Polydopamine in Sensing Applications, Polymers 15 (2023) 3712.
[16] Z.Q. Liu, X. Yang, Q. Zhang, TURBISCAN: history, development, application to colloids and dispersions, Adv. Mater. Res. 936 (2014) 1592–1596.
[17] R. Malivindi, F. Patitucci, S. Prete, M. Dattilo, A.E. Leonetti, N. Scigliano, O. I. Parisi, F. Puoci, Efficacy and safety assessment of PIMIN050 raft-forming system as medical device based on Citrus sinensis and Crassostrea gigas for the management of gastroesophageal reflux disease, J. Drug Deliv. Sci. Technol. 78 (2022) 103986.
[18] S. Moneshwaran, D. Macrin, N. Kanagathara, An unprecedented global challenge, emerging trends and innovations in the fight against COVID-19: A comprehensive review, Int. J. Biol. Macromol. (2024) 131324.
[19] G.M. Morris, R. Huey, W. Lindstrom, M.F. Sanner, R.K. Belew, D.S. Goodsell, A. J. Olson, AutoDock4 and AutoDockTools4: Automated docking with selective receptor flexibility, J. Comput. Chem. 30 (2009) 2785–2791.
[20] M.S. Muthu, S.-S. Feng, Pharmaceutical stability aspects of nanomedicines, Nanomedicine 4 (2009) 857–860.
[21] O.I. Parisi, M. Dattilo, F. Patitucci, R. Malivindi, S. Delbue, P. Ferrante, S. Parapini, R. Galeazzi, M. Cavarelli, F. Cilurzo, Design and development of plastic antibodies against SARS-CoV-2 RBD based on molecularly imprinted polymers that inhibit in vitro virus infection, Nanoscale 13 (2021) 16885–16899.
[22] O.I. Parisi, F. Francomano, M. Dattilo, F. Patitucci, S. Prete, F. Amone, F. Puoci, The evolution of molecular recognition: From antibodies to molecularly imprinted polymers (MIPs) as artificial counterpart, J. Funct. Biomater. 13 (2022) 12.
[23] E.F. Pettersen, T.D. Goddard, C.C. Huang, G.S. Couch, D.M. Greenblatt, E.C. Meng, T.E. Ferrin, UCSF Chimera—a visualization system for exploratory research and analysis, J. Comput. Chem. 25 (2004) 1605–1612.
[24] A. Raziq, A. Kidakova, R. Boroznjak, J. Reut, A. Öpik, V. Syritski, Development of a portable MIP-based electrochemical sensor for detection of SARS-CoV-2 antigen, Biosens. Bioelectron. 178 (2021) 113029.
[25] S.H. Shahcheraghi, J. Ayatollahi, A.A. Aljabali, M.D. Shastri, S.D. Shukla, D. K. Chellappan, N.K. Jha, K. Anand, N.K. Katari, M. Mehta, An overview of vaccine development for COVID-19, Ther. Deliv. 12 (2021) 235–244.
[26] A.N. Stephen, S.R. Dennison, M. Holden, S.M. Reddy, Rapid sub-nanomolar protein determination in serum using electropolymerized molecularly imprinted polymers (E-MIPs), Analyst 148 (2023) 5476–5485.
[27] C. Tian, K. Kasavajhala, K.A. Belfon, L. Raguette, H. Huang, A.N. Migues, J. Bickel, Y. Wang, J. Pincay, Q. Wu, ff19SB: amino-acid-specific protein backbone parameters trained against quantum mechanics energy surfaces in solution, J. Chem. Theory Comput. 16 (2019) 528–552.
[28] S.S. Toussi, J.L. Hammond, B.S. Gerstenberger, A.S. Anderson, Therapeutics for COVID-19, Nat. Microbiol. 8 (2023) 771–786.
[29] W.H.O. WHO, Classif. omicron (B. 1. 1. 529): SARS-CoV-2 Var. Concern. (2021).
[30] W.H.O. WHO, Corona Dis. (COVID-19) Epidemiol. Updates Mon. Oper. Updates (2024).
[31] J. Zhou, L. Wang, X. Liu, Y. Gai, M. Dong, C. Wang, M.M. Ali, M. Ye, X. Yu, L. Hu, Glycan-Imprinted Nanoparticle as Artificial Neutralizing Antibody for Efficient HIV-1 Recognition and Inhibition, Nano Lett. 24 (2024) 4423–4432.